ACS APPLIED MATERIALS & INTERFACES

Research Article

www.acsami.org

Improve First-Cycle Efficiency and Rate Performance of Layered-Layered $Li_{1.2}Mn_{0.6}Ni_{0.2}O_2$ Using Oxygen Stabilizing Dopant

Jinfeng Li,[†,⊥] Chun Zhan,[‡,⊥] Jun Lu,*[,‡] Yifei Yuan,[‡,§] Reza Shahbazian-Yassar,[§] Xinping Qiu,*[,†] and Khalil Amine*[,‡]

[†]Key Laboratory of Organic Optoelectronics and Molecular Engineering, Department of Chemistry, Tsinghua University, Beijing 100084, China

[‡]Chemical Sciences and Engineering Division, Argonne National Laboratory, Argonne, Illinois 60439, United States

[§]Department of Materials Science and Engineering, Michigan Technological University, 1400 Townsend Drive, Houghton, Michigan 49931, United States

ABSTRACT: The poor first-cycle Coulombic efficiency and rate performance of the Li-rich layered-layered oxides are associated with oxygen gas generation in the first activation charging and sluggish charge transportation along the layers. In this work, we report that barium doping improves the first-cycle efficiency of Li-rich layered-layered $Li_{1.2}Mn_{0.6}Ni_{0.2}O_2$ via suppression of the oxidation of O^{2-} ions in the first charging. This effect can be attributed to the stabilizing effect of the barium cations on the oxygen radical intermediates generated during the oxidation of O^{2-}. Meanwhile, because the stabilized oxygen radicals likely facilitate the charge transportation in the layered-layered structure, the barium-doped $Li_{1.2}Mn_{0.6}Ni_{0.2}O_2$ exhibits significant improvement in rate performance. Stabilizing the oxygen radicals could be a promising strategy to improve the electrochemical performance of Li-rich layered-layered oxides.

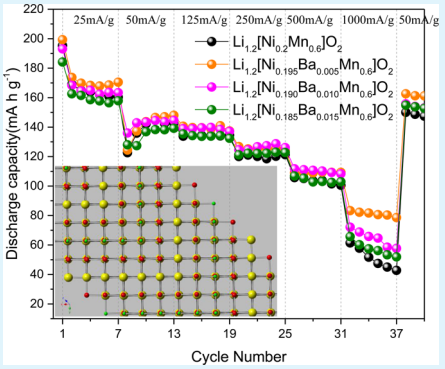

KEYWORDS: *layered-layered $Li_{1.2}Mn_{0.6}Ni_{0.2}O_2$, barium doping, lithium ion battery, oxygen releasing, stabilizing oxygen radicals*

1. INTRODUCTION

In cathode materials of lithium ion batteries, increasing the Li-to-TM (transition metal) ratio to higher than one has been extensively pursued in the past years in order to boost the energy density of lithium ion batteries. One of the simplest Li-rich layered oxides, Li_2MnO_3, which can be rewritten as $Li[Li_{1/3}Mn_{2/3}]O_2$, allows access of two Li ions per Mn ion, i.e., a theoretical capacity of 458 mAh/g.[1] In actual cell tests, however, only about 350 mAh/g capacity can be achieved in the first charge to 4.7 V, and the first-cycle Coulombic efficiency is lower than 60%.[2] Because the Mn(IV) ions are unlikely to be oxidized to higher valence in the octahedral coordination environment in pristine Li_2MnO_3, the O^{2-} ions in the Li_2MnO_3 are oxidized to O_2 to facilitate the extraction of Li^+ ions in the first charge.[3] In the first discharge, however, the reinsertion of Li ions is coupled with the reduction of Mn(IV) to Mn(III), exhibiting completely different electrochemical behaviors.[4−7] The poor first-cycle Coulombic efficiency can thus be attributed to the irreversible capacity loss due to the O_2 releasing, resulting in one Li ion inserting back after the extracting of two Li ions in the first cycle.[6,8,9] On the other hand, The poor rate performance of the Li_2MnO_3 can be attributed to the lack of Mn^{4+}/Mn^{3+} redox couples for the electron hopping[10] and/or the formation of a thick solid-electrolyte interface layer due to the oxygen released.[11,12]

The structural integration of the Li_2MnO_3 with a layered metal oxide $LiMO_2$ (M = Mn, Co, Ni, etc.) provides a practical approach to exploit the high Li/TM ratio of Li_2MnO_3.[13−15] The so-called Li-rich layered-layered oxides ($xLi_2MnO_3\cdot(1-x)LiMO_2$, designated as LLO thereafter), derive high capacity (~250 mAh/g) from the Li_2MnO_3 domains and passable electron and lithium ion conductivity from the $[MO_2]_n$ units.[16−18] A representative LLO is $Li_{1.2}Mn_{0.6}Ni_{0.2}O_2$ ($0.5Li_2MnO_3\cdot0.5LiMn_{0.5}Ni_{0.5}O_2$). Its first-charge voltage profile exhibits a sloping region at potentials lower than 4.4 V corresponding to the oxidation of Ni(II) to Ni(IV), followed by a plateau at about 4.5 V that is consistent with the activation of the Li_2MnO_3 domains with the removal of Li^+ and O_2.[4,13,19−23] In spite of the improvement in the electrochemical performance owing to the contribution of $LiMO_2$, the rate performance and the first-cycle efficiency of LLO still cannot meet the requirements for practical application.[24−30] Further breakthrough of the LLO requires the direct suppressing of the O_2 releasing from the Li_2MnO_3.[8,9,19]

In this work, barium ion was investigated as an oxygen stabilizing dopant to improve both the rate performance and the first-cycle efficiency of the Li-rich layered-layered $Li_{1.2}Mn_{0.6}Ni_{0.2}O_2$. We found that an extremely low concentration of the Ba (x = 0.005 in $Li_{1.2}Ba_xNi_{0.2-x}Mn_{0.6}O_2$) yielded superior electrochemical performance compared to

Received: May 19, 2015
Accepted: June 29, 2015
Published: June 29, 2015

DOI: 10.1021/acsami.5b04343
ACS Appl. Mater. Interfaces 2015, 7, 16040−16045

$Li_{1.2}Mn_{0.6}Ni_{0.2}O_2$. The oxygen generation in the first charge was effectively suppressed by the Ba doping, and over 50% of the initial capacity was retained a discharge rate up to 4 C. The mechanism of the improvement is likely related to the stabilized O^{2-} in the Li_2MnO_3 domains due to the bonding between Ba and O.

2. EXPERIMENTAL METHODS

2.1. Material Synthesis and Characterization. Both $Li_{1.2}Mn_{0.6}Ni_{0.2}O_2$ and $Li_{1.2}Ba_xNi_{0.2-x}Mn_{0.6}O_2$ (x = 0.005, 0.01, and 0.015) were synthesized by a coprecipitation method. 10 mL of $NH_3\cdot H_2O$ (29.8%) was added to a solution with the required amount of $MnCl_2$, $Ni(NO_3)_2\cdot 6H_2O$, and $BaCl_2$ under stirring, and then the solution was transferred to a 50 mL autoclave with a Teflon liner. The autoclave was maintained at 200 °C for 6 h and then air cooled to room temperature. The resulting dark powders were collected by filtration and washed with distilled water and ethanol before drying overnight at 75 °C in a vacuum oven. The precursor was then mixed with Li_2CO_3 thoroughly and then sintered in air at 900 °C for 24 h.

High-resolution powder X-ray diffraction (HRPXRD) patterns of the samples were collected at the 11-BM beamline of the Advanced Photon Source, Argonne National Laboratory. The samples were loaded into kapton capillaries and rotated during the experiment at a rate of 90 rotations per second. The data were collected for 2θ of 0.5° to about 40° with a step size of 0.001° and a time of 0.2 s per step. The HRPXRD traces were collected with 12 silicon (111) crystal analyzers, which increase detector efficiency, reduce the angular range to be scanned, and allow rapid acquisition of data. A silicon and alumina NIST standard (ratio of 1/3 Si to 2/3 Al_2O_3) was used to calibrate the instrument and to determine and refine the wavelength used in the experiment, which is about 0.413 839 Å. High-angle annular dark field (HAADF) imaging of the samples was carried out inside an aberration-corrected JEOL JEM-ARM200CF scanning transmission electron microscopy (STEM) instrument. A 22 mrad probe convergence angle was used to capture all the HAADF images at a collection angle of 90–370 mrad.

2.2. Electrochemical Tests. The undoped and doped cathode materials were tested in 2032 coin cells. The cathodes consisted of 85 wt % active material, 5 wt % poly(vinylidene fluoride) as a binder, and 10 wt % carbon black as the conducting agent. After being fully mixed with *N*-methylpyrrolidinone solution, the slurry was cast uniformly onto an aluminum foil with a 200 μm doctor blade. After drying at 75 °C in air for 4 h and another 12 h under vacuum, the laminates were compressed by a rolling press and then punched into 1.6 cm^2 disk electrodes. The 2032 coin cells were assembled with Celgard 2325 separators and GenII electrolyte (1.2 M $LiFP_6$ in 3:7 ratio of ethylene carbonate and ethyl methyl carbonate) in an argon-filled glovebox. The cells were initially activated in the first charge at constant current/constant voltage (CC/CV). The cells were first charged galvanostatically at 0.1 C (calculated for an anticipated capacity of 250 mAh g^{-1}) to the cutoff voltage of 4.7 V and then charged potentiostatically at 4.8 V for 20 h. The following discharges and charges were controlled between 2.0 and 4.8 V with gradually increasing rates of 0.1, 0.2, 0.4, 1, 2, and 4 C, then back to 0.2 C to determine the rate performance of the electrodes. Cyclic voltammatry of the electrodes was carried out with a Solartron Model 1470E Eight Channel Potentiostat/Galvanostat using a scan rate of 0.05 mV s^{-1} within the potential range from 4.8 to 2 V vs Li^+/Li.

3. RESULTS

3.1. Structure and Morphology. The $Li_{1.2}Ba_xNi_{0.2-x}Mn_{0.6}O_2$ ($0.005 \le x \le 0.015$) was prepared by a solid-state reaction of the coprecipitated carbonates of Ni, Mn, and Ba with Li_2CO_3. Figure 1 presents the XRD patterns of as-prepared $Li_{1.2}Ba_xNi_{0.2-x}Mn_{0.6}O_2$ along with the undoped material, which correspond primarily to the O3 type layered structure (space group $R\bar{3}m$) with Bragg positions labeled as

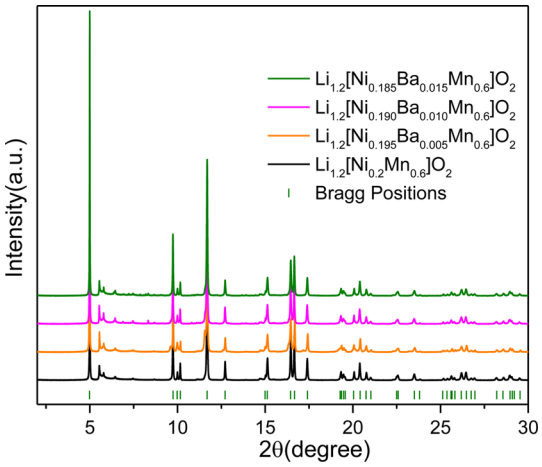

Figure 1. High-resolution powder X-ray diffraction (HRPXRD) patterns of $Li_{1.2}Ba_xNi_{0.2-x}Mn_{0.6}O_2$ ($0 \le x \le 0.015$).

the green bars at the bottom. The unindexed peaks around 2θ = 6°–8° can be assigned to the superstructure reflections consistent with the $LiMn_6$ cation ordering that occurs in the transition metal layers of the Li_2MnO_3.[16] The XRD patterns were refined with $R\bar{3}m$ space group by the Fullprof suite. The lattice parameters of the samples with different Ba doping concentrations are listed in Table 1, revealing that the Ba

Table 1. Lattice Parameters Calculated from the Refinements of the XRD Patterns of the $Li_{1.2}Ba_xNi_{0.2-x}Mn_{0.6}O_2$ ($0 \le x \le 0.015$)

x in $Li_{1.2}Ba_xNi_{0.2-x}Mn_{0.6}O_2$	$a = b$ (Å)	c (Å)	c/a	cell volume (Å^3)
0	2.8566(3)	14.2470(7)	4.987	100.685(1)
0.005	2.8534(1)	14.2692(0)	5.001	100.614(3)
0.010	2.8583(0)	14.2571(5)	4.988	100.873(6)
0.015	2.8567(8)	14.2510(5)	4.989	100.723(5)

doping does not obviously influence the crystal structure of the $Li_{1.2}Ni_{0.2}Mn_{0.6}O_2$, probably due to the low concentration of Ba doping. In addition, the c/a ratio is slightly increased by the Ba doping when x = 0.005, which is likely due to the replacement of smaller Ni^{2+} ions by the larger Ba^{2+} ions.

The unchanged crystal structure was further confirmed by HAADF imaging of the samples, which has been reported to efficiently detect the signals of heavy elements such as Mn.[31] Figure 2a,b shows HAADF images of $Li_{1.2}Ni_{0.2}Mn_{0.6}O_2$ and $Li_{1.2}Ba_{0.015}Ni_{0.185}Mn_{0.6}O_2$ particles, respectively, taken along the [4–4–1] zone axis. A series of bright rows can be observed on both images, which are correlated with transition metal (Mn and/or Ni) rich layers due to their high atomic number. The lattice spacing for the Ba-doped and Ba-free particles is measured to be 0.20 nm, matching the $d_{\{104\}}$ of $Li_{1.2}Ni_{0.2}Mn_{0.6}O_2$ very well. The atomic configuration for $Li_{1.2}Ni_{0.2}Mn_{0.6}O_2$ agrees with the [4–4–1] zone axis model shown in Figure 2c, confirming the experimental projection to be [4–4–1] for both Ba-doped and Ba-free particles. This finding indicates that the crystalline structure of this cathode material is well maintained after Ba doping. It is also notable that the atomic column brightness varies at different sites. Because the atomic model demonstrates that Li, Ni, and Mn atoms are all well aligned along the [4–4–1] axis, the uneven

DOI: 10.1021/acsami.5b04343
ACS Appl. Mater. Interfaces 2015, 7, 16040–16045

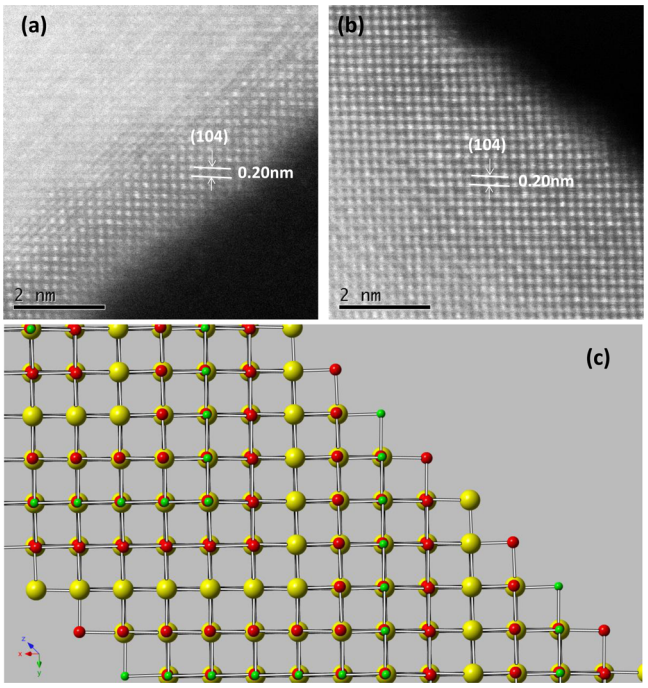

Figure 2. Atomic-resolution HAADF-STEM images of $Li_{1.2}Ba_xNi_{0.2-x}Mn_{0.6}O_2$ with (a) $x = 0$ and (b) $x = 0.015$ at high magnification taken along [4−4−1] zone axis; (c) [4−4−1] zone axis atomic model showing the configuration of $Li_{1.2}Ni_{0.2}Mn_{0.6}O_2$, where green balls indicate Li^+, red for O, and yellow for Mn and Ni. Under such a zone axis, all four atomic species are well aligned parallel to the viewing direction.

brightness distribution implies the existence of Li−Ni disorder at the nanoscale.

3.2. Electrochemical Performance. Figure 3 compares the first charge−discharge curves of the $Li_{1.2}Ba_xNi_{0.2-x}Mn_{0.6}O_2$ with varying barium content. The electrodes were charged at constant current/constant voltage, with galvanostatic charging

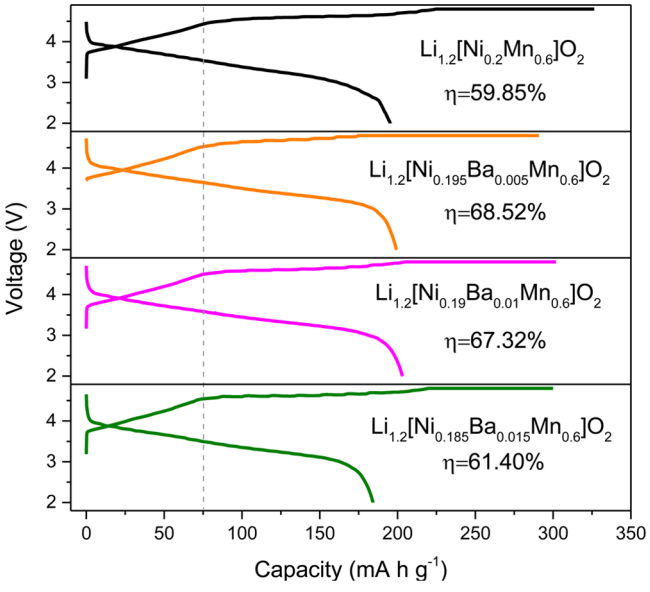

Figure 3. First-cycle charge−discharge profiles of $Li_{1.2}Ba_xNi_{0.2-x}Mn_{0.6}O_2$ ($0 \le x \le 0.015$) electrodes with the current density of 25 mA/g.

up to 4.8 V and then potentiostatic charging at 4.8 V for 20 h. A low current density at 25 mA g^{-1} was applied for the activation of the Li_2MnO_3 domains. The voltage curves in Figure 3 demonstrate the characteristic sloping and plateau formation of Li-rich layered-layered oxides. The capacity of the $Li_{1.2}Ba_xNi_{0.2-x}Mn_{0.6}O_2$ samples in the sloping region, which corresponds to the oxidation of Ni^{2+} to Ni^{4+}, slightly decreases when the Ba content (x) is increased from 0 to 0.015. This capacity decline is can be attributed to the replacement of the electrochemically active Ni^{2+} ions by the inactive Ba^{2+} ions, or because Ba^{2+} ions likely inhibit the diffusion of Li ions due to their large radius. On the other hand, the capacity of the plateau region above 4.5 V significantly decreases with Ba doping. As mentioned earlier, the plateau above 4.5 V is related to the oxidation of O^{2-} to O_2 gas, and thus the decrease in the capacity above 4.5 V indicates that the O_2 releasing reaction is suppressed by the Ba^{2+} doping. The corresponding first-cycle Coulombic efficiencies (η) of the undoped and Ba-doped samples are listed in Figure 3. As shown in the figure, the first-cycle Coulombic efficiency increases from 59.85% to 68.52% with Ba content of $x = 0.005$, but decreases to 67.32% and 61.40% when $x = 0.010$ and 0.015, respectively. It is interesting that the Ba-doped cathode with the lowest Ba concentration exhibits the highest η, which will be explained in detail in the Discussion section.

The impact of the Ba doping on the O^{2-} oxidation reaction is clearly demonstrated in the cyclic voltammograms shown in Figure 4. The potential of the $Li_{1.2}Ba_xNi_{0.2-x}Mn_{0.6}O_2$ electrodes

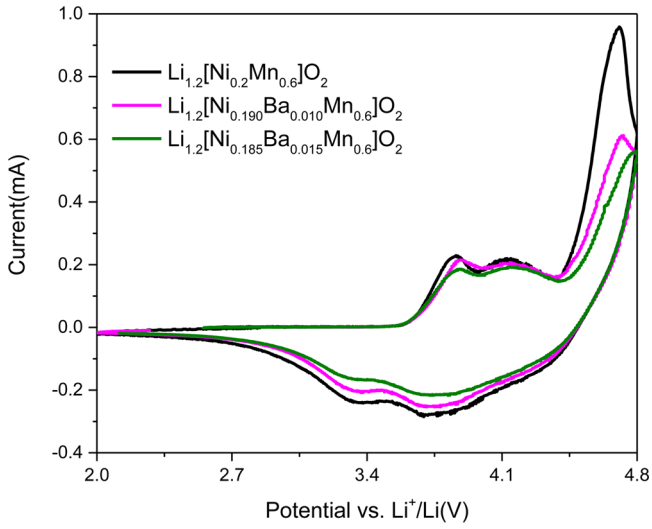

Figure 4. Cyclic voltammatry curves of $Li_{1.2}Ba_xNi_{0.2-x}Mn_{0.6}O_2$ ($0 \le x \le 0.015$) electrodes using a scan rate of 0.05 mV s^{-1} within the potential range from 4.8 to 2 V vs Li^+/Li.

was cycled between 4.8 and 2 V with a low scan rate of 0.05 mV s^{-1} to distiguish the redox reactions occurring at different potentials. The two oxidation peaks at 3.7 and 4.1 V correlate to the oxidation of Ni(II) to Ni(III) and Ni(III) to Ni(IV), respectively. The coresponding reduction peaks occur at about 3.4 and 3.7 V during the reverse cyclic voltammetry sweep. No oxidation peak of the Mn(III) appeared, confirming that most Mn ions in the compound are at the +4 oxidation state. The sharp peak at about 4.7 V can be attributed to the expected oxidation of the O^{2-} when more than one Li ion is removed from the $Li_{1.2}Ba_xNi_{0.2-x}Mn_{0.6}O_2$. Note that when a small portion of Ni^{2+} ions is replaced by Ba^{2+} ions, the oxidation peak

DOI: 10.1021/acsami.5b04343
ACS Appl. Mater. Interfaces 2015, 7, 16040−16045

at about 4.7 V shifts to higher potential and the peak current decreases by about 50%. These changes reveal that the oxidation of O^{2-} is significantly suppressed by the Ba doping, which is consistent with the first-cycle charge−discharge profile in Figure 3.

The rate performance of the $Li_{1.2}Ba_xNi_{0.2-x}Mn_{0.6}O_2$ electrodes is plotted in Figure 5. The electrodes were activated under

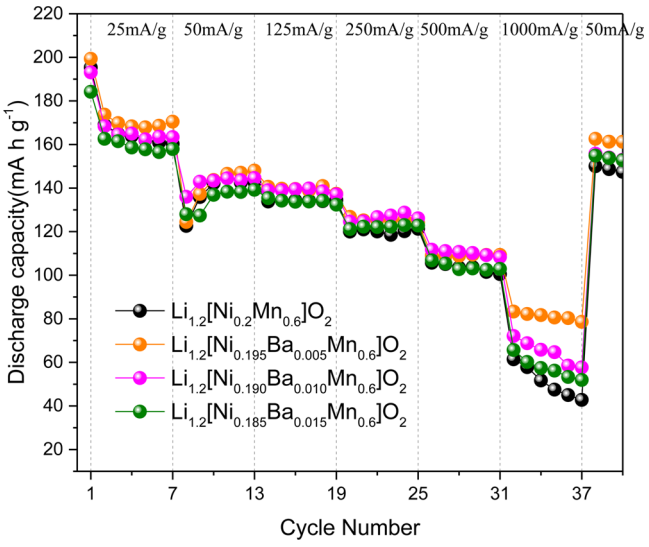

Figure 5. Rate performance of $Li_{1.2}Ba_xNi_{0.2-x}Mn_{0.6}O_2$ ($0 \le x \le 0.015$).

the CC−CV mode for the first cycle, and then cycled between 2.0 and 4.8 V at a series of increasing rates (0.1, 0.2, 0.5, 1, 2, and 4 C) for six cycles at each rate, and then the rate was reduced to 0.2 C. In the activation cycle, the discharge capacities of the $Li_{1.2}Ba_xNi_{0.2-x}Mn_{0.6}O_2$ electrodes were similar when $0 \le x \le 0.010$. In the subsequent cycles with increasing rate, the discharge capacities of all the electrodes declined gradually due to the polarization in the cell. For the rate of 1 C or lower, the capacities of Ba-doped electrodes were slightly higher than that of the undoped electrode. When cycled intensively at higher current densities, the rate performance due to the Ba doping increased more significantly. In particular, when cycled at 4 C, the discharge capacity of the $Li_{1.2}Ni_{0.2}Mn_{0.6}O_2$ cathode declined rapidly from 60 to 40 mAh g^{-1} within 6 cycles, which is less than 35% of the initial discharge capacity and can be related to the poor electronic conductivity associated with the Mn^{4+} ions. On the contrary, the discharge capacity of the $Li_{1.2}Ba_{0.005}Ni_{0.195}Mn_{0.6}O_2$ remained at about 80 mAh g^{-1} when cycled at 4 C, which is nearly double the capacity of the undoped electrode after 6 cycles at 4 C. These results clearly show that Ba doping at low concentration facilitates fast charge transport in the Li-rich layered-layered structure. The rate performance of the doped cathode with the lowest Ba content ($x = 0.005$) is superior to that of the other samples, which is similar to the first-cycle efficiency results shown in Figure 3. The correlation between the low-concentration Ba doping and the improvement in first-cycle efficiency and rate performance will be discussed in the following section.

4. DISCUSSION

The O_2 release accompanying the Li^+ ion extraction from the Li_2MnO_3 can be expressed as

$$Li_2MnO_3 \rightarrow 2Li^+ + MnO_2 + \frac{1}{2}O_2 + 2e^-$$

The oxidation of O^{2-} to O_2 provides two electrons to compensate for the two Li^+ ions extracted. This O_2 releasing reaction is irreversible in the cell, and thus only one Li^+ can reinsert into the MnO_2 accompanying the reduction of Mn^{4+} to Mn^{3+}:

$$Li^+ + MnO_2 + e^- \rightarrow LiMnO_2$$

The above delithiation−lithiation mechanism of the Li_2MnO_3 explains the poor first-cycle efficiency of the Li-rich layered oxide materials. As shown in Figures 3 and 4, the O_2 releasing reaction during the initial activation is noticeably suppressed by the Ba doping, which gives rise to the improved first-cycle efficiency. As reported in the literature,[4] the O_2 releasing reaction likely occurs with the oxygen radicals ($O_2^{\bullet-}$ or $O^{\bullet-}$) as the intermediate. Because of the large radius and thus low positive charge density of the Ba^{2+} ion, we hypothesize that Ba ions are capable of stabilizing the oxygen radicals, similar to the mechanism of the stability of the BaO_2.[32] Therefore, the Ba doping reduces the amount of O_2 released in the first charge. Moreover, the electrons generated due to the Li^+ removal remain in the cathode as unpaired electron in the oxygen radicals because of the suppressing of the O_2 releasing. As a result, the electron density in the cathode can be increased, leading to higher electron conductivity, which could be one of the possible reasons for the improvement in the rate performance of the Ba-doped $Li_{1.2}Ba_{0.005}Ni_{0.195}Mn_{0.6}O_2$. Nevertheless, owing to the large radius of the Ba^{2+} ions, it is unlikely that the $Li_{1.2}Ni_{0.2}Mn_{0.6}O_2$ structure can host a high content of barium. For the $Li_{1.2}Ba_xNi_{0.2-x}Mn_{0.6}O_2$ samples with x values higher than 0.005, only a part of the Ba^{2+} ions may replace the Ni^{2+} ions in the lattices, while the other part stays at the surface of the particles and may block the Li ion transportation at the electrolyte/electrode interface. This behavior explains why the Ba doping at the lowest concentration yields the highest first-cycle Coulombic efficiency and the best rate performance.

5. CONCLUSIONS

In this work, doping with Ba^{2+} has been shown to improve significantly the first-cycle efficiency and rate performance of the Li-rich layered-layered oxide $Li_{1.2}Ni_{0.2}Mn_{0.6}O_2$. The improved electrochemical performance is proposed to correlate with the suppressed O_2 releasing reaction in the first charge or the activation process. This reaction could be attributed to the stabilizing effect of the barium cations on the oxygen radical intermediates generated during the oxidation of O^{2-}. The detailed mechanism study is still ongoing, but this work suggests great opportunities to improve the Li-rich layered-layered oxide toward practical applications via stabilizing the oxygen in the structure.

AUTHOR INFORMATION

Corresponding Authors

*Jun Lu. E-mail: junlu@anl.gov. Tel.: +1 630-252-4485.

*Xinping Qiu. E-mail: qiuxp@mail.tsinghua.edu.cn. Tel.: +86 10-6279-2716.

*Khalil Amine. E-mail: amine@anl.gov. Tel.: +1 630-252-3838.

Author Contributions

⊥These authors contributed equally.

Notes

The authors declare no competing financial interest.

DOI: 10.1021/acsami.5b04343
ACS Appl. Mater. Interfaces 2015, 7, 16040−16045

■ ACKNOWLEDGMENTS

J. Li and X. Qiu were supported by the National Key Project on Basic Research (2015CB251104, 2013CB934000), National International Science and Technology Cooperation Project (2012DFG61480), China-Germany Electric Vehicle Project (2011AA11A290), China-US Electric Vehicle Project (2010DFA72760), and Beijing Natural Science Foundation (2120001). C. Zhan, J. Lu, and K. Amine were supported by the Center for Electrical Energy Storage, an Energy Frontier Research Center funded by the U.S. Department of Energy, Office of Science, Office of Basic Energy Sciences. Use of the Advanced Photon Source was supported by the U.S. Department of Energy, Office of Science, Office of Basic Energy Sciences, under Contract No. DE-AC02-06CH11357. Y. Yuan and R. Shahbazian-Yassar acknowledge the financial support from the National Science Foundation (Awards CMMI-1200383 and DMR-1410560), and partial funding from Argonne National Laboratory under subcontract No. 4F31422. This work made use of the JEOL JEM-ARM200CF in the Electron Microscopy Service (Research Resources Center, UIC). The acquisition of the UIC JEOL JEM-ARM200CF was supported by a MRI-R2 grant from the National Science Foundation [DMR-0959470].

■ REFERENCES

(1) Wang, R.; He, X.; He, L.; Wang, F.; Xiao, R.; Gu, L.; Li, H.; Chen, L. Atomic Structure of Li_2MnO_3 after Partial Delithiation and Re-Lithiation. *Adv.Energy Mater.* **2013**, *3* (10), 1358−1367.

(2) Yu, D. Y. W.; Yanagida, K.; Kato, Y.; Nakamura, H. Electrochemical Activities in Li_2MnO_3. *J. Electrochem. Soc.* **2009**, *156* (6), A417−A424.

(3) Gao, Y.; Ma, J.; Wang, X.; Lu, X.; Bai, Y.; Wang, Z.; Chen, L. Improved Electron/Li-ion Transport and Oxygen Stability of Mo-doped Li_2MnO_3. *J. Mater. Chem. A* **2014**, *2* (13), 4811−4818.

(4) Hong, J.; Lim, H.-D.; Lee, M.; Kim, S.-W.; Kim, H.; Oh, S.-T.; Chung, G.-C.; Kang, K. Critical Role of Oxygen Evolved from Layered Li−Excess Metal Oxides in Lithium Rechargeable Batteries. *Chem. Mater.* **2012**, *24* (14), 2692−2697.

(5) Pasero, D.; McLaren, V.; de Souza, S.; West, A. R. Oxygen Nonstoichiometry in Li_2MnO_3: An Alternative Explanation for Its Anomalous Electrochemical Activity. *Chem. Mater.* **2005**, *17* (2), 345−348.

(6) Armstrong, A. R.; Robertson, A. D.; Bruce, P. G. Overcharging Manganese Oxides: Extracting Lithium Beyond Mn^{4+}. *J. Power Sources* **2005**, *146* (1−2), 275−280.

(7) Robertson, A. D.; Bruce, P. G. Mechanism of Electrochemical Activity in Li_2MnO_3. *Chem. Mater.* **2003**, *15* (10), 1984−1992.

(8) Wang, F.; Chang, Z.; Wang, X.; Wang, Y.; Chen, B.; Zhu, Y.; Wu, Y. Composites of Porous Co_3O_4 Grown on Li_2MnO_3 Microspheres as Cathode Materials for Lithium Ion Batteries. *J. Mater. Chem. A* **2015**, *3* (9), 4840−4845.

(9) Wang, F.; Xiao, S.; Chang, Z.; Li, M.; Wu, Y.; Holze, R. Coaxial $LiCoO_2$@ Li_2MnO_3 Nanoribbon as a High Capacity Cathode for Lithium Ion Batteries. *Int. J. Electrochem. Sci.* **2014**, *9*, 6182−6190.

(10) Kunduraci, M.; Al-Sharab, J. F.; Amatucci, G. G. High-Power Nanostructured $LiMn_{2-x}Ni_xO_4$ High-Voltage Lithium-Ion Battery Electrode Materials: Electrochemical Impact of Electronic Conductivity and Morphology. *Chem. Mater.* **2006**, *18* (15), 3585−3592.

(11) Singh, G.; Thomas, R.; Kumar, A.; Katiyar, R.; Manivannan, A. Electrochemical and Structural Investigations on ZnO Treated $0.5Li_2MnO_3{\cdot}0.5\ LiMn_{0.5}Ni_{0.5}O_2$ Layered Composite Cathode Material for Lithium Ion Battery. *J. Electrochem. Soc.* **2012**, *159* (4), A470−A478.

(12) Kang, S.-H.; Thackeray, M. M. Enhancing the rate capability of high capacity $xLi_2MnO_3{\cdot}(1\text{-}x)LiMO_2$ (M=Mn, Ni, Co) electrodes by Li−Ni−PO4 treatment. *Electrochem. Commun.* **2009**, *11* (4), 748−751.

(13) Lu, Z.; Dahn, J. R. Understanding the Anomalous Capacity of $Li/Li[Ni_xLi_{(1/3-2x-3)}Mn_{(2/3-x/3)}]O_2$ Cells Using In Situ X-Ray Diffraction and Electrochemical Studies. *J. Electrochem. Soc.* **2002**, *149* (7), A815−A822.

(14) Thackeray, M. M.; Kang, S. H.; Johnson, C. S.; Vaughey, J. T.; Hackney, S. A. Comments on the Structural Complexity of Lithium-Rich $Li_{1+x}M_{1-x}O_2$ Electrodes (M=Mn, Ni, Co) for Lithium Batteries. *Electrochem. Commun.* **2006**, *8* (9), 1531−1538.

(15) Xu, J.; Dou, S.; Liu, H.; Dai, L. Cathode Materials for Next Generation Lithium Ion Batteries. *Nano Energy* **2013**, *2* (4), 439−442.

(16) Thackeray, M. M.; Kang, S.-H.; Johnson, C. S.; Vaughey, J. T.; Benedek, R.; Hackney, S. Li_2MnO_3-Stabilized $LiMO_2$ (M= Mn, Ni, Co) Electrodes for Lithium-Ion Batteries. *J. Mater. Chem.* **2007**, *17* (30), 3112−3125.

(17) Yu, H.; Zhou, H. High-Energy Cathode Materials (Li_2MnO_3-$LiMO_2$) for Lithium-Ion Batteries. *J. Phys. Chem. Lett.* **2013**, *4* (8), 1268−1280.

(18) Lu, Z.; MacNeil, D. D.; Dahn, J. R. Layered Cathode Materials $Li[Ni_xLi_{(1/3-2x/3)}Mn_{(2/3-x/3)}]O_2$ for Lithium-Ion Batteries. *Electrochem. Solid-State Lett.* **2001**, *4* (11), A191−A194.

(19) Wang, C.-C.; Manthiram, A. Influence of Cationic Substitutions on the First Charge and Reversible Capacities of Lithium-Rich Layered Oxide Cathodes. *J. Mater. Chem. A* **2013**, *1* (35), 10209−10217.

(20) Xiang, X.; Knight, J. C.; Li, W.; Manthiram, A. Understanding the Effect of Co^{3+} Substitution on the Electrochemical Properties of Lithium-Rich Layered Oxide Cathodes for Lithium-Ion Batteries. *J. Phys. Chem. C* **2014**, *118* (38), 21826−21833.

(21) Lei, C. H.; Bareño, J.; Wen, J. G.; Petrov, I.; Kang, S. H.; Abraham, D. P. Local Structure and Composition Studies of $Li_{1.2}Ni_{0.2}Mn_{0.6}O_2$ by Analytical Electron Microscopy. *J. Power Sources* **2008**, *178* (1), 422−433.

(22) Kang, S.-H.; Sun, Y. K.; Amine, K. Electrochemical and Ex Situ X-Ray Study of $Li(Li_{0.2}Ni_{0.2}Mn_{0.6})O_2$ Cathode Material for Li Secondary Batteries. *Electrochem. Solid-State Lett.* **2003**, *6* (9), A183−A186.

(23) Kang, S.-H.; Johnson, C. S.; Vaughey, J. T.; Amine, K.; Thackeray, M. M. The Effects of Acid Treatment on the Electrochemical Properties of $0.5\ Li_2MnO_3{\bullet}0.5\ LiNi_{0.44}Co_{0.25}Mn_{0.31}O_2$ Electrodes in Lithium Cells. *J. Electrochem. Soc.* **2006**, *153* (6), A1186−A1192.

(24) van Bommel, A.; Krause, L. J.; Dahn, J. R. Investigation of the Irreversible Capacity Loss in the Lithium-Rich Oxide $Li[Li_{1/5}Ni_{1/5}Mn_{3/5}]O_2$. *J. Electrochem. Soc.* **2011**, *158* (6), A731−A735.

(25) Singh, G.; Thomas, R.; Kumar, A.; Katiyar, R. S. Electrochemical Behavior of Cr- Doped Composite $Li_2MnO_3{\cdot}LiMn_{0.5}Ni_{0.5}O_2$ Cathode Materials. *J. Electrochem. Soc.* **2012**, *159* (4), A410−A420.

(26) Xu, B.; Fell, C. R.; Chi, M.; Meng, Y. S. Identifying Surface Structural Changes in Layered Li-Excess Nickel Manganese Oxides in High Voltage Lithium Ion Batteries: A Joint Experimental and Theoretical Study. *Energy Environ. Sci.* **2011**, *4* (6), 2223−2233.

(27) Liu, J.; Reeja-Jayan, B.; Manthiram, A. Conductive Surface Modification with Aluminum of High Capacity Layered $Li[Li_{0.2}Mn_{0.54}Ni_{0.13}Co_{0.13}]O_2$ Cathodes. *J. Phys. Chem. C* **2010**, *114* (20), 9528−9533.

(28) Liu, G.-B.; Liu, H.; Wang, Y.; Shi, Y.-F.; Zhang, Y. The Electrochemical Properties of Fe-and Ni-cosubstituted Li_2MnO_3 via Combustion Method. *J. Solid State Electrochem.* **2013**, *17* (9), 2437−2444.

(29) Zhao, T.; Li, L.; Chen, R.; Wu, H.; Zhang, X.; Chen, S.; Xie, M.; Wu, F.; Lu, J.; Amine, K. Design of Surface Protective layer of LiF/FeF_3 Nanoparticles in Li-rich Cathode for High-Capacity Li-Ion Batteries. *Nano Energy* **2015**, *15* (0), 164−176.

(30) Ye, D.; Ozawa, K.; Wang, B.; Hulicova-Jurcakova, D.; Zou, J.; Sun, C.; Wang, L. Capacity-Controllable Li-Rich Cathode Materials for Lithium-Ion Batteries. *Nano Energy* **2014**, *6* (0), 92−102.

(31) Yuan, Y.; Nie, A.; Odegard, G. M.; Xu, R.; Zhou, D.; Santhanagopalan, S.; He, K.; Asayesh-Ardakani, H.; Meng, D. D.; Klie, R. F.; Johnson, C.; Lu, J.; Shahbazian-Yassar, R. Asynchronous Crystal

DOI: 10.1021/acsami.5b04343
ACS Appl. Mater. Interfaces 2015, 7, 16040−16045

Cell Expansion during Lithiation of K^+-Stabilized α-MnO_2. *Nano Lett.* **2015**, *15* (5), 2998−3007.
(32) Middleburgh, S. C.; Lagerlof, K. P. D.; Grimes, R. W. Accommodation of Excess Oxygen in Group II Monoxides. *J. Am. Ceram. Soc.* **2013**, *96* (1), 308−311.

DOI: 10.1021/acsami.5b04343
ACS Appl. Mater. Interfaces 2015, 7, 16040−16045